Arab J Sci Eng (2014) 39:7097–7107
DOI 10.1007/s13369-014-1336-8

RESEARCH ARTICLE - COMPUTER ENGINEERING AND COMPUTER SCIENCE

New Set of Gegenbauer Moment Invariants for Pattern Recognition Applications

Khalid M. Hosny

Received: 31 May 2013 / Accepted: 31 January 2014 / Published online: 28 August 2014

Abstract A new set of Gegenbauer moment invariants is proposed for pattern recognition applications. These moment invariants are expressed as a linear combination of geometric moment invariants where the later are invariants under translation, scaling and rotation of the image they describe. The invariance of Gegenbauer moments is tested by using different binary- and gray-level images. The obtained results show the accuracy of the new set of Gegenbauer moment invariants.

Keywords Orthogonal moments · Gegenbauer moment invariants · Geometric moment invariants · Classification

الخلاصة

يقترح هذا البحث مجموعة جديدة من عزوم Gegenbauer اللامتغيرة لتطبيقات التعرف على الأنماط. وهذه العزوم اللامتغيرة يتم تمثيلها بوصفها تركيبة خطية من العزوم الهندسية اللامتغيرة حيث الأخيرة هي عزوم متغيرة طبقا للإزاحة والتحجيم الدوران للصورة التي تصفها. وقد تم اختبار تغير عزوم Gegenbauer باستخدام مختلف الصور الثنائية اللون والرمادية. وأظهرت النتائج التي تم الحصول عليها دقة مجموعة عزوم Gegenbauer اللامتغيرة الجديدة.

1 Introduction

The concept of moment invariants of images was introduced by Hu [1] where he derived a set of nine moment invariants by using geometric moments of the input image. Hu's moment invariants are used in different image processing and pattern recognition applications. Due to the limitations in the image reconstruction capabilities of geometric moments, Teague [2] used orthogonal polynomials to compute image moments instead of monomials as in the case of Hu. Legendre and Zernike moments are examples of these orthogonal polynomials. Teh and Chain [3] reported that orthogonal moments are used to represent images with the minimum of information redundancy.

Since Gegenbauer polynomials are orthogonal [4], these polynomials are used to represent digital images with the minimum of information redundancy. In addition to these attractive properties, orthogonal Gegenbauer polynomials are characterized by a scaling parameter $\alpha > -0.5$, where specific values of this parameter produce different sets of other orthogonal polynomials. Pawlak [5] shows that this scaling parameter provides a trade-off between global and local image features.

Recently, Hosny [6] proposed the theme of image representation by using highly accurate orthogonal Gegenbauer moments. In his work, Hosny confirmed the robustness of orthogonal Gegenbauer moments against different kinds of noise. To the author's best knowledge, there is no work dealing with the derivation and computation of Gegenbauer moment invariants with respect to translation, scaling and rotation.

Recognition of images and shapes based on their invariant features and the discrimination between similar images are very important themes. The accuracy of the discrimination process mainly depends on the accurate computation of the invariant features of the images.

Kan and Srinath [7] used orthogonal Zernike moment invariants for invariant classification of alphanumeric characters of different sizes. Jazzar and Muhammed [8] proposed a multimodal biometric system with high security level based on finger and palm print. The verification/identification is performed by fusing features form different finger and palm

K. M. Hosny (✉)
Department of Information Technology, Faculty of Computers and Informatics, Zagazig University, Zagazig, Egypt
e-mail: k_hosny@yahoo.com

prints. The features are extracted using Zernike moment invariants.

Chong et al. [9] introduced a new set of translation and scale invariants of Legendre moments based on Legendre polynomials. The descriptors remain unchanged for translated, elongated, contracted and reflected non-symmetrical, as well as symmetrical images. Rao et al. [10] used exact Legendre moments and support vector machine in content-based image retrieval.

Pang et al. [11] used enhanced pseudo-Zernike moment invariants in face recognition. Kanan et al. [12] used adaptively weighted patch pseudo-Zernike moments of a single image per person for face recognition. Moreover, Kanan and Faez [13] studied the optimal selection of pseudo-Zernike moment invariants features for face recognition.

In this paper, a new set of accurate orthogonal Gegenbauer moment invariants (GMIs) is presented. These GMIs are expressed as a linear combination of regular moment invariants (RMIs) where the later are invariant under translation, scaling and rotation of the image they describe. RMIs are computed as a linear combination of the central moments. A fast algorithm is applied to accelerate the computation process, where the computational elapsed times are greatly reduced.

The rest of the paper is organized as follows: In Sect. 2, a brief overview of orthogonal Gegenbauer polynomials and their moments is presented. The proposed method for derivation of Gegenbauer moment invariants is described in Sect. 3. Numerical experiments are discussed in Sect. 4. The conclusion is presented in Sect. 5. Finally, a list of references is presented.

2 Orthogonal Gegenbauer Polynomials

Gegenbauer polynomial of the nth order is defined as follows [4]:

$$G_n^{(\alpha)}(x) = \sum_{k=0}^{\lfloor \frac{n}{2} \rfloor} (-1)^k \frac{\Gamma\,(n-k+\alpha)}{k\,!(n-2k)!\Gamma(\alpha)}\,(2x)^{n-2k} \tag{1}$$

The operator $\lfloor n/2 \rfloor$ is defined as:

$$\left\lfloor \frac{n}{2} \right\rfloor = \begin{cases} (n-1)/2, & n \text{ is odd} \\ n/2, & n \text{ is even} \end{cases} \tag{2}$$

The explicit expansion of $G_n^{(\alpha)}(x)$ is rewritten as follows:

$$G_n^{(\alpha)}(x) = \sum_{\substack{k=0 \\ n-k=\text{even}}}^{n} B_{n,k}^{(\alpha)}\, x^k \tag{3}$$

With the coefficient matrix $B_{n,k}^{(\alpha)}$ defined as:

$$B_{n,k}^{(\alpha)} = (-1)^{\frac{n-k}{2}} \frac{\Gamma\left(\alpha + \frac{n+k}{2}\right)\, 2^k}{k\,!\left(\frac{n-k}{2}\right)!\Gamma(\alpha)} \tag{4}$$

The first five Gegenbauer functions are defined in a matrix form as follows:

$$\begin{pmatrix} G_0^{(\alpha)} \\ G_1^{(\alpha)} \\ G_2^{(\alpha)} \\ G_3^{(\alpha)} \\ G_4^{(\alpha)} \end{pmatrix} = \begin{pmatrix} 1 & 0 & 0 & 0 & 0 \\ 0 & 2\alpha & 0 & 0 & 0 \\ -\alpha & 0 & 2(\alpha)_2 & 0 & 0 \\ 0 & -2(\alpha)_2 & 0 & \frac{4}{3}(\alpha)_3 & 0 \\ \frac{1}{2}(\alpha)_2 & 0 & -2(\alpha)_3 & 0 & \frac{2}{3}(\alpha)_4 \end{pmatrix} \times \begin{pmatrix} 1 \\ x \\ x^2 \\ x^3 \\ x^4 \end{pmatrix} \tag{5}$$

with:

$$(\alpha)_n = \alpha\,(\alpha+1)\,(\alpha+2)\ldots(\alpha+n-1) \tag{6}$$

The low-order Gegenbauer polynomials are plotted and displayed in Figs. 1 and 2. Direct computation of the coefficient matrix $B_{n,m}^{(\alpha)}$ by using Eqs. (4) is time-consuming where the computational process includes evaluation of factorial terms and Gamma function, $\Gamma(\cdot)$, for each value of n and m. Based on the Gamma function properties, a set of recurrence relations is derived to easily compute $B_{n,m}^{(\alpha)}$ recursively. Gamma functions and factorial terms are not included in these recurrence relations as follows:

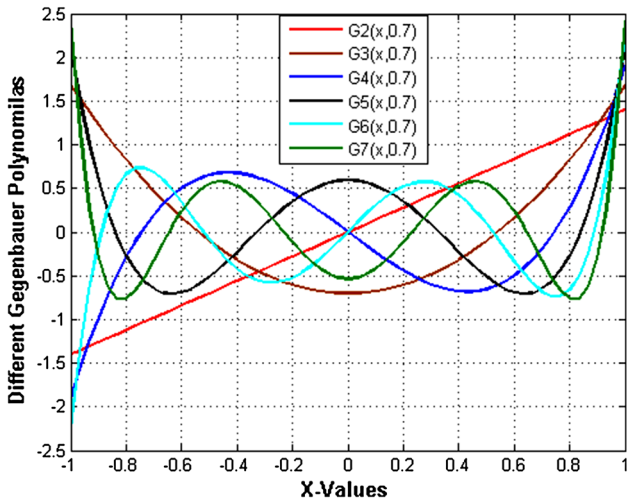

Fig. 1 Gegenbauer polynomials of low orders plotted and graphically displayed

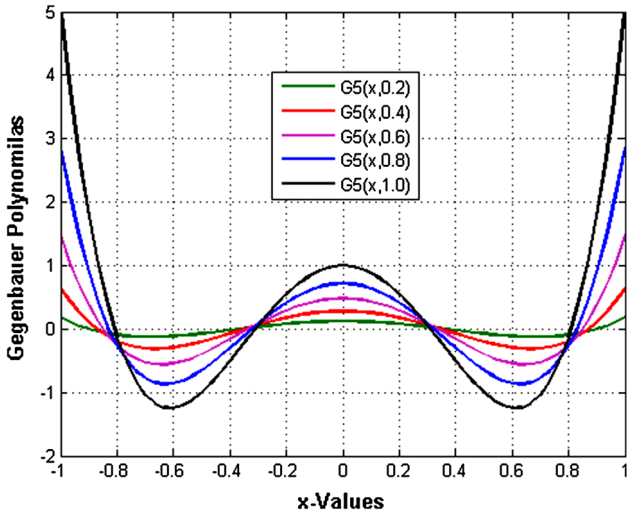

Fig. 2 Graphical representation of the fifth orders Gegenbauer polynomials with different values of the scaling parameter $\alpha > -0.5$

$$B_{0,0}^{(\alpha)} = 1, \tag{7}$$

$$B_{n,n}^{(\alpha)} = \frac{2\,(\alpha + n - 1)}{n} B_{n-1,n-1}^{(\alpha)}, \tag{8}$$

$$B_{n,n-t}^{(\alpha)} = -\frac{(n-t+1)\,(n-t+2)}{2t\,\left(\alpha + n - \frac{t}{2}\right)} B_{n,n-t+2}^{(\alpha)}. \tag{9}$$

with $t = 2, 4, 6, \ldots, n$. The following pseudo-code is helpful for the reader to easily understand this computational process.

$B_{0,0}^{(\alpha)} = 1$

for n = 1 : Max

$$B_{n,n}^{(\alpha)} = \frac{2(\alpha + n - 1)}{n} B_{n-1,n-1}^{(\alpha)}$$

endfor

for n = 2 : Max

for m = n − 2 : −2 : mod(p, 2)

$$B_{n,n-m}^{(\alpha)} = -\frac{n\,(n-1)}{4\,(\alpha + n - 1)} B_{n,m+2}^{(\alpha)}$$

endfor

endfor

Gegenbauer polynomials are orthogonal over the square $[-1 \le x \le 1] \times [-1 \le y \le 1]$ and satisfy the following orthogonality property:

$$\int_{-1}^{1} G_n^{(\alpha)}(x) G_m^{(\alpha)}(x) w^{(\alpha)}(x) \mathrm{d}x = C_n(\alpha)\delta_{nm} \tag{10}$$

With the weight function:

$$w^{(\alpha)}(x) = \left(1 - x^2\right)^{\alpha - 0.5} \tag{11}$$

The Kronecker symbol, δ_{nm}, and the normalization constant, $C_n(\alpha)$, are defined as follows:

$$C_n(\alpha) = \frac{2\pi\,\Gamma\,(n + 2\alpha)}{2^{2\alpha} n!\,(n + \alpha)\;[\Gamma(\alpha)]^2} \tag{12}$$

The time-consuming computational process for normalization constant evaluation is avoided by using the recurrence relations [6]. Orthogonal 2D Gegenbauer moments of order $(n,\ m)$ are defined as follows:

$$A_{n,m} = \frac{1}{C_n(\alpha) C_m(\alpha)} \int_{-1}^{1} \int_{-1}^{1} f(x, y) G_n^{(\alpha)}(x)\; G_m^{(\alpha)} \times (y) w^{(\alpha)}(x) w^{(\alpha)}(y) \mathrm{d}x \mathrm{d}y \tag{13}$$

The indices $n,\ m$ are nonnegative integers.

3 Gegenbauer Moment Invariants (GMIs)

Equation (13) is rewritten where GMIs are expressed in terms of RMIs. Substituting Eq. (3) into (13) yields:

$$\hat{A}_{n,m} = \frac{1}{C_n(\alpha) C_m(\alpha)} \sum_{\substack{k=0 \\ n-k=\text{even}}}^{n} \sum_{\substack{\ell=0 \\ m-\ell=\text{even}}}^{m} B_{n,k}^{(\alpha)} B_{m,\ell}^{(\alpha)} \times \int_{-1}^{1} \int_{-1}^{1} x^{n-2k} \left(1 - x^2\right)^{\alpha - 0.5} \times y^{m-2\ell} \left(1 - y^2\right)^{\alpha - 0.5} f\,(x, y)\,\mathrm{d}x\;\mathrm{d}y \tag{14}$$

Assume the function $h(x, y)$ is defined as:

$$h\,(x, y) = \left(1 - x^2\right)^{\alpha - 0.5} \left(1 - y^2\right)^{\alpha - 0.5} f(x, y) \tag{15}$$

Equation (14) is rewritten as follows:

$$\hat{A}_{n,m} = \frac{1}{C_n(\alpha) C_m(\alpha)} \sum_{\substack{k=0 \\ n-k=\text{even}}}^{n} \sum_{\substack{\ell=0 \\ m-\ell=\text{even}}}^{m} \times B_{n,k}^{(\alpha)} B_{m,\ell}^{(\alpha)} \int_{-1}^{1} \int_{-1}^{1} x^{n-2k} y^{m-2\ell} h(x, y) \mathrm{d}x\;\mathrm{d}y \tag{16}$$

The integration in Eq. (16) represents the geometric moments of the image intensity function $h(x,\ y)$. Therefore, Eq. (16) could be rewritten as follows:

$$\hat{A}_{n,m} = \frac{1}{C_n(\alpha) C_m(\alpha)} \sum_{\substack{k=0 \\ n-k=\text{even}}}^{n} \sum_{\substack{\ell=0 \\ m-\ell=\text{even}}}^{m} \times B_{n,k}^{(\alpha)} B_{m,\ell}^{(\alpha)} \mathrm{RMI}_{(n-2k),(m-2\ell)} \tag{17}$$

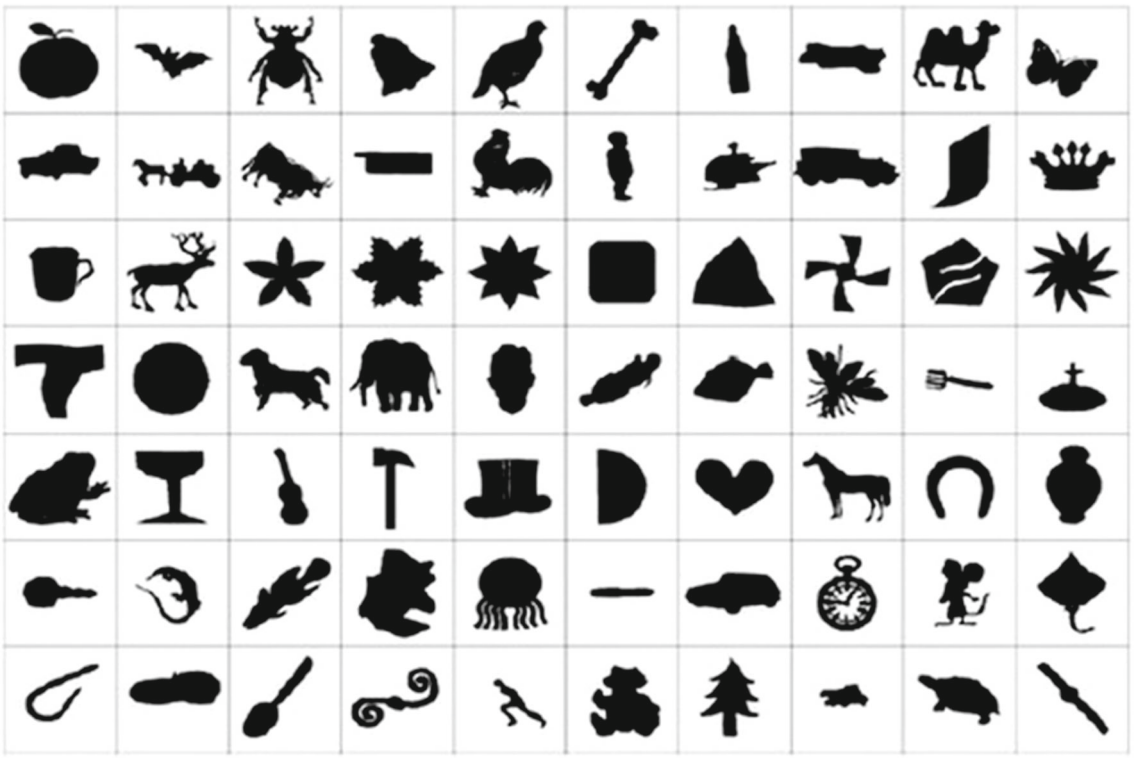

Fig. 3 Displaying of all shapes of the MPEG-7 CE-Shape-1 dataset

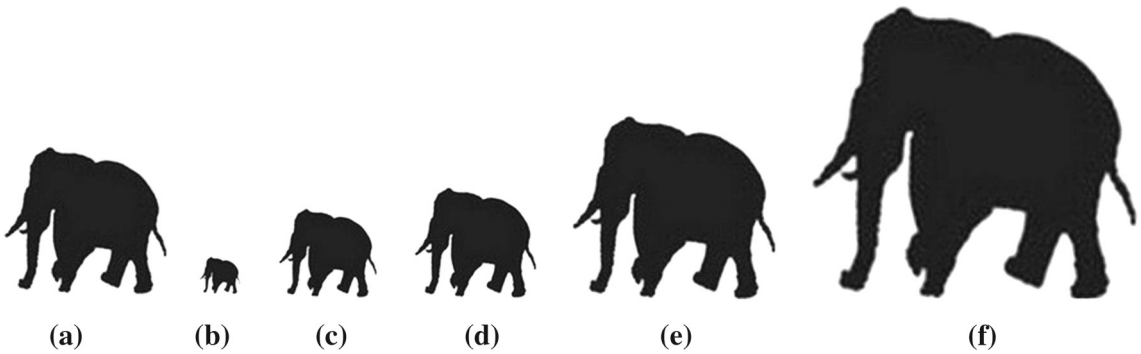

Fig. 4 Testing the invariance to scale by using the binary shape of "Elephant"

where $\mathrm{RMI}_{p,q}$ are the regular moment invariants of order $(p+q)$.

3.1 Regular Moment Invariants (RMIs)

Regular moment invariants of image/shape are the features that remain unchanged if that image/shape undergoes any combination of translation, scaling, and rotation.

Translation invariance is achieved through the central moments. These moments are defined by shifting the coordinate system with the image centroid $(x_0,\ y_0)$. This centroid is defined for the new intensity function as follows:

$$x_0 = \frac{\sum_{i=1}^{N}\sum_{j=1}^{N} x_i h\left(x_i, y_j\right)}{\sum_{i=1}^{N}\sum_{j=1}^{N} h\left(x_i, y_j\right)},$$
$$y_0 = \frac{\sum_{i=1}^{N}\sum_{j=1}^{N} y_j h\left(x_i, y_j\right)}{\sum_{i=1}^{N}\sum_{j=1}^{N} h\left(x_i, y_j\right)} \tag{18}$$

The central moments are:

$$\mu_{pq} = \int_{-\infty}^{\infty}\int_{-\infty}^{\infty} (x-x_0)^p (y-y_0)^q h(x,y)\,\mathrm{d}x\mathrm{d}y \tag{19}$$

Central moments are directly computed without any prior knowledge of the geometric moments. Invariance to uniform scaling of factor α could be achieved through the cancelation

Table 1 Scale invariance of the binary shape "Elephant"

	Original image	Contracted images			Expanded images	
	200 × 200	50 × 50	120 × 120	150 × 150	250 × 2500	400 × 400
I(3)	0.3647	0.3646	0.3647	0.3647	0.3647	0.3647
I(4)	−0.0446	−0.0446	−0.0446	−0.0446	−0.0446	−0.0446
I(5)	0.2927	0.2924	0.2927	0.2927	0.2927	0.2927
I(6)	−0.0305	−0.0301	−0.0304	−0.0304	−0.0304	−0.0304
I(7)	0.0308	0.0307	0.0308	0.0308	0.0308	0.0308
I(8)	−0.0407	−0.0407	−0.0407	−0.0407	−0.0407	−0.0407
I(9)	0.0003	0.0001	0.0003	0.0003	0.0003	0.0003
I(10)	−0.0521	−0.0517	−0.0521	−0.0521	−0.0521	−0.0521
I(11)	0.0432	0.0429	0.0432	0.0432	0.0432	0.0432
I(12)	−0.2446	−0.2436	−0.2445	−0.2445	−0.2446	−0.2446
I(13)	0.0610	0.0608	0.0609	0.0610	0.0610	0.0610
I(14)	0.0751	0.0752	0.0751	0.0751	0.0751	0.0751

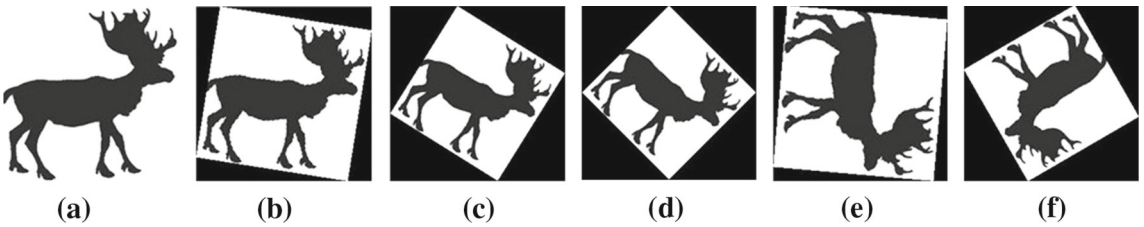

Fig. 5 Testing the invariance to rotation by using the binary shape of "deer"

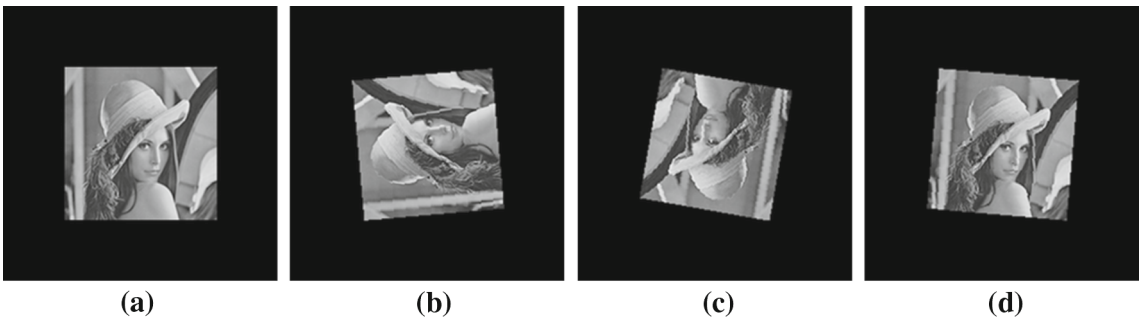

Fig. 6 Testing the invariance to rotation by using the gray-level image of "Lena"

of the scaling factors by setting μ'_{00} equal to the unity. The scale-translation invariant moments are

$$\mu'_{pq} = \frac{\mu_{pq}}{\mu_{00}^{\lambda}},\ \lambda = \frac{p+q+2}{2} \tag{20}$$

The third kind of transformation is the rotation through an angle θ. This angle is usually measured counterclockwise about the coordinate origin. The rotation transformation is represented by the following form:

$$M_{pq}^{rot} = \int_{-\infty}^{\infty}\int_{-\infty}^{\infty} (x\cos\theta + y\sin\theta)^p \times (y\cos\theta - x\sin\theta)^q\, h(x,y)\mathrm{d}x\,\mathrm{d}y, \tag{21}$$

By using the binomial theorem with Eq. (21) and using the scale-translation invariant moments instead of the geometric moments, the set of regular moment invariants are defined as follows:

$$\mathrm{RMI}_{pq} = \frac{1}{\mu_{00}^{\lambda}} \sum_{k=0}^{p}\sum_{m=0}^{q} \binom{p}{k}\binom{q}{m} (-1)^m (\sin\theta)^{k+m} \times (\cos\theta)^{p+q-k-m}\ \mu_{p-k+m,q-m+k} \tag{22}$$

Table 2 Rotation invariance of the binary shape "deer"

	Original image	Rotation angle				
		9°	32°	45°	95°	150°
I(3)	−0.2912	−0.2902	−0.2908	−0.2902	−0.2906	−0.2901
I(4)	0.0009	−0.0008	−0.0002	0.0007	0.0005	0.0003
I(5)	−0.2209	−0.2204	−0.2217	−0.2203	−0.2216	−0.2219
I(6)	0.0004	0.0003	0.0001	0.0005	0.0006	0.0008
I(7)	0.0090	0.0081	0.0089	0.0084	0.0081	0.0086
I(8)	−0.0027	−0.0025	−0.0025	−0.0028	−0.0023	−0.0023
I(9)	0.0024	0.0019	0.0018	0.0021	0.0020	0.0023
I(10)	0.1091	0.1083	0.1094	0.1080	0.1084	0.1088
I(11)	0.0183	0.0179	0.0186	0.0180	0.0181	0.0185
I(12)	0.0776	0.0769	0.0771	0.0765	0.0770	0.0770
I(13)	−0.0263	−0.0241	−0.0240	−0.0243	−0.0239	−0.0239
I(14)	−0.0572	−0.0570	−0.0566	−0.0568	−0.0570	−0.0570

Table 3 Rotation invariance of the gray-level image "Lena"

	Original image	Rotated image #1	Rotated image #2	Rotated image #3
I(3)	−0.2032	−0.2026	−0.2034	−0.2028
I(4)	−0.0001	0.0001	0.0003	0.0001
I(5)	−0.1669	−0.1658	−0.1657	−0.1655
I(6)	0.0402	0.0412	0.0406	0.0396
I(7)	−0.0056	−0.0063	−0.0055	−0.0054
I(8)	0.0140	0.0144	0.0138	0.0134
I(9)	−0.0002	−0.0012	−0.0009	−0.0008
I(10)	0.0795	0.0802	0.0799	0.0796
I(11)	0.0049	0.0061	0.0052	0.0055
I(12)	−0.0562	−0.0542	−0.0557	−0.0549
I(13)	−0.0111	−0.0113	−0.0106	−0.0110
I(14)	0.0299	0.0304	0.0301	0.0302

With a rotation angle defined as:

$$\theta = \frac{1}{2}\tan^{-1}\left(\frac{2\mu_{11}}{\mu_{20}-\mu_{02}}\right) \tag{23}$$

3.2 Accurate Computation of RMIs

Computation of RMIs required the computation of central moments as the main counterpart of the whole process. Central moments defined by Eq. (19) could be computed by using the following form:

$$\mu_{pq} = \sum_{i=1}^{M}\sum_{j=1}^{N} T_{pq}\left(x_i, y_j\right)\ h\left(x_i, y_j\right), \tag{24}$$

where

$$T_{pq}(x_i, y_j) = \int_{x_i-\frac{\Delta x_i}{2}}^{x_i+\frac{\Delta x_i}{2}}\int_{y_j-\frac{\Delta y_j}{2}}^{y_j+\frac{\Delta y_j}{2}} (x-x_0)^p\ (y-y_0)^q dxdy \tag{25}$$

Writing Eq. (25) in a separable form and replace it in Eq. (24) yields:

$$\mu_{pq} = \sum_{i=1}^{M}\sum_{j=1}^{N} I_p\,(i)\ I_q\,(j)\ h\left(x_i, y_j\right) \tag{26}$$

where

$$I_p\,(i) = \int_{x_i-\frac{\Delta x_i}{2}}^{x_i+\frac{\Delta x_i}{2}} (x-x_0)^p\,dx = \frac{1}{p+1}\left[(U_{i+1}-x_0)^{p+1} - (U_i-x_0)^{p+1}\right] \tag{27}$$

$$I_q\,(j) = \int_{y_j-\frac{\Delta y_j}{2}}^{y_j+\frac{\Delta y_j}{2}} (y-y_0)^q\,\mathrm{d}y = \frac{1}{q+1}\left[(V_{j+1}-y_0)^{q+1} - (V_j-y_0)^{q+1}\right] \tag{28}$$

The upper and lower limits of the integration in the Eqs. (27, 28) are defined as in [14,15]. A fast algorithm could be applied to accelerate this computational process where the central moments of order $(p+q)$ could be computed in two steps by successive computation of the 1D qth order moments for each row. This methodology proved to be very efficient and successfully used in the case of 2D and 3D images [16–19].

4 Experimental Results

The validity and efficiency of the proposed method are analyzed in the three subsections of this section. The first subsection is concerned with the accuracy where the validity of the proposed method is proved. A set of numerical experiments is conducted with different images from selected image databases. These images are scaled with different factors and rotated with different angles. The results of these experiments clearly show that GMIs are accurate invariants under different aforementioned transformations.

Discrimination power of the GMIs is discussed in the second subsection. The proposed set of orthogonal GMIs is used in classifying similar images from different standard databases with high classification ratio.

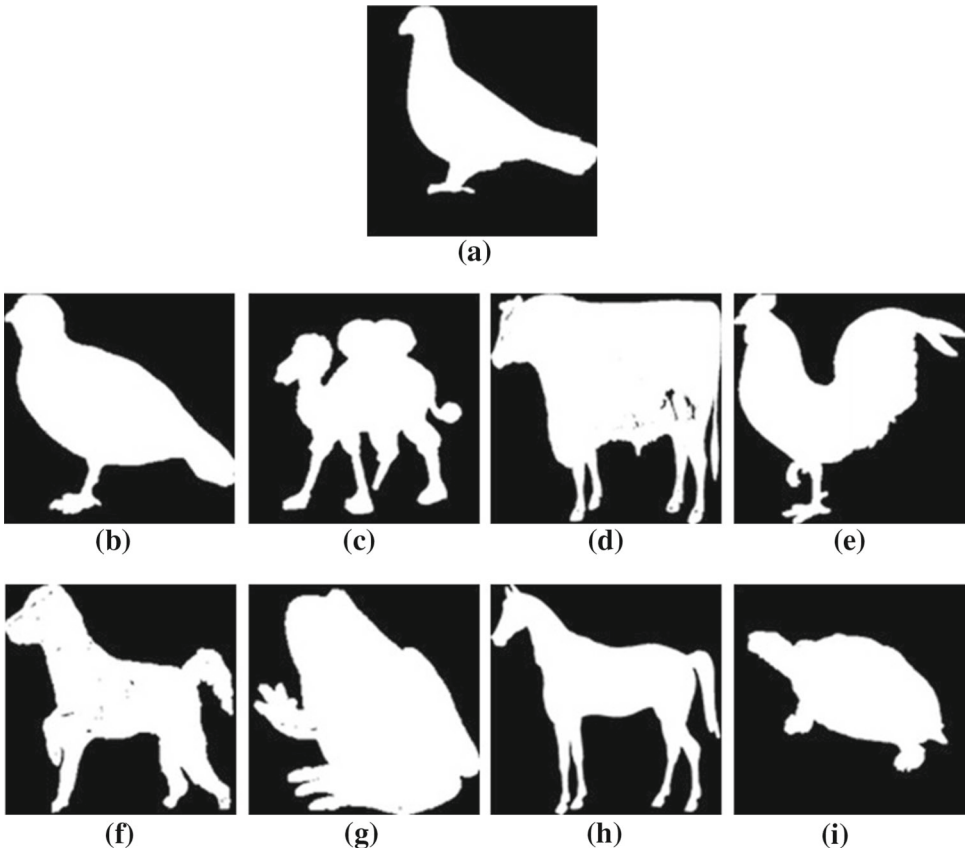

Fig. 7 Displaying the selected binary shapes from MPEG7_CE-Shape-1_Part_B dataset

Table 4 Euclidean distance and correlation coefficients for Binary shapes of selected animals

	Query shape	Selected shapes of animals							
	V_A	V_B	V_C	V_D	V_E	V_F	V_G	V_H	V_I
d_1		0.1126	0.3181	0.2998	0.2964	0.1916	0.4187	0.3287	0.2994
d_2		0.9808	0.8362	0.8589	0.8466	0.9350	0.7562	0.7955	0.8717

According to the extreme importance of the CPU elapsed time especially when dealing with large image and shape databases, the third subsection is devoted to evaluate the computational performance on different databases. A comparison of the computational elapsed CPU times of different methods is presented.

4.1 Accuracy

The accuracy of GMIs is evaluated through a series of numerical experiments. To easily analyze the accuracy of the GMIs, 1D vector of these invariants is constructed from the computed set of independent 2D orthogonal Gegenbauer moments. For a maximum moment order *Max*, the total number of independent regular and Gegenbauer moments is equal to $(Max+1)(Max+1)/2$. The conversion process could be done by using the conversion code [14].

GMIs of the second, third and fourth orders are used in all the conducted numerical experiments. In the first experiment, a binary image of "Elephant" is selected from the MPEG-7 CE-Shape-1 database [20]. This database consists of 1,400 shapes, which are grouped into 70 categories with 20 shapes each as shown in Fig. 3. This database is commonly used to test different kinds of shape descriptors [21].

The 200×200 binary image of "Elephant" as displayed in Fig. 4a is uniformly scaled with the ratios 25, 60, 75, 125 and 200 %. The scaled images of the "Elephant" are displayed in Fig. 4b–f, respectively.

Low orders of GMIs are computed for the original binary image and the scaled images. The obtained results are shown in Table 1. It is clear that the numerical values of low- order GMIs are almost identical for the original, expanded and contracted images. The results of this numerical experiment ensure the accuracy of the GMIs.

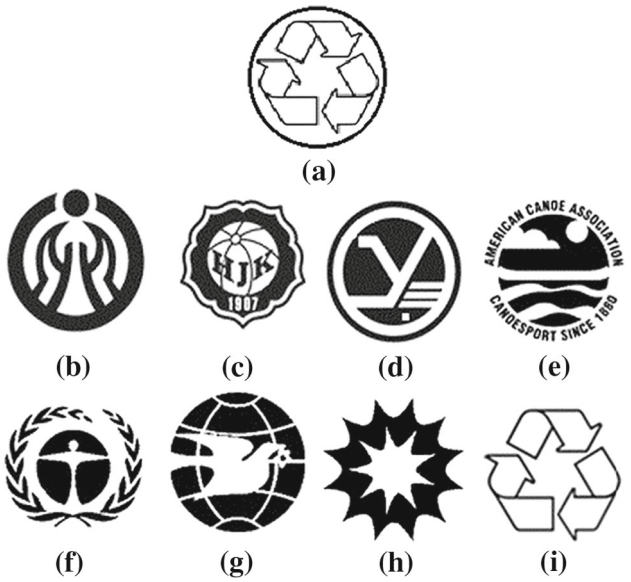

Fig. 8 Displaying the selected gray-level images of trademarks

Rotational invariance is an essential property for pattern classification and recognition. A numerical experiment is conducted to evaluate the invariance of GMIs with respect to rotation. The binary image of "deer" as displayed in Fig. 5a is selected from the MPEG-7 CE-Shape-1 database. This image is rotated with different angles ranging from acute to very large angles. The rotated images with their rotation angles are displayed in Fig. 5b–f.

An additional numerical experiment for rotational invariance is conducted. The standard gray-level image of "Lena" as displayed in Fig. 6 a is used in this experiment. The original gray-level image of Lena is padded with zeros and then rotated with three different angles. The rotated images are displayed in Fig. 6b–d, respectively.

Low-order GMIs are computed for these transformed images where the obtained numerical values are listed in Tables 2 and 3, respectively. The numerical values are very similar, which ensure the invariance of Gegenbauer moments with respect to rotation. Based on the results of these numerical experiments, the accuracy of the GMIs is absolutely obvious.

4.2 Discrimination Power

The discrimination between similar images and shapes is an essential process in many applications such as retrieving images based on their content. To achieve this goal, classifiers are used where their discrimination power is highly dependent on the accuracy of the features being used. Gegenbauer moment invariants of lower orders are computed and stored in feature vectors. In this section, numerical experiments were conducted where the Euclidean distance and the correlation coefficients are used to measure the similarity between the different images. These measures are defined by using the following form [22]:
Euclidean distance:

$$d_1(S,T) = \sqrt{\sum_{i=1}^{ns}(S_i - T_i)^2} \tag{29}$$

Correlation coefficients:

$$d_2(S,T) = \frac{\sum_{i=1}^{ns} S_i T_i}{\left|\sum_{i=1}^{ns} S_i S_i\right|^{0.5} \left|\sum_{i=1}^{ns} T_i T_i\right|^{0.5}} \tag{30}$$

The vectors of the selected features, S and T, have the length ns. The value of the measure, d_1, tends to be 0 for the case of the two equal vectors, while d_2 tends to be 1.

In the first numerical experiment, a group of binary shapes of animals were selected from different groups of the MPEG7_CE-Shape-1_Part_B [20]. The correlation coefficient between the low-order GMIs of the two binary shapes is used as a quantitative measure for the similarity between the different shapes where the maximum correlation between shapes will be achieved by the shapes from the same group.

The selected binary shapes, "bird_18," "bird_2," "camel_3," "cattle_10," "chicken_4," "dog_4," "frog_19," "horse_6," and "turtle_1" are displayed in Fig. 7 a–i, respectively. In this experiment, the GMIs of lower orders for the selected shapes are computed and stored in the feature vectors, V_A, V_B, V_C, V_D, V_E, V_F, V_G, V_H and V_I, respectively. The similarity between the binary shape A and all of the other selected shapes was determined, and the obtained results are shown in Table 4. Based on these results, the maximum value of the correlation coefficients was found between feature vectors, V_A and V_B, which represent two shapes from the same group.

An additional numerical experiment was conducted where a group of gray-level images of trademarks were used [23]. The images of the selected trademarks are displayed in

Table 5 Euclidean distance and correlation coefficients for gray-level images of selected trademarks

	Query logo	Selected gray-level images of logos							
	V_A	V_B	V_C	V_D	V_E	V_F	V_G	V_H	V_I
d_1		0.3188	0.3184	0.3992	0.4703	0.3668	0.3184	0.4146	0.0717
d_2		0.8262	0.8195	0.6740	0.5004	0.7371	0.8421	0.6419	0.9912

Fig. 9 Collection of the 40 faces (ORL-faces)

Fig. 10 Collection of the COIL-20 objects

Fig. 8a–i, respectively. The GMIs of lower orders for the selected images are computed and stored in the feature vectors, V_A, V_B, V_C, V_D, V_E, V_F, V_G, V_H and V_I, respectively. The similarity between the selected trademark image, A, and other selected images was determined. The obtained results are shown in Table 5. Based on these results, the maximum value of the correlation coefficients was found between feature vectors, V_A and V_I. This result is completely consistent with the naked eye's observation. The results of the conducted experiments ensure the discrimination power of the GMIs.

4.3 Computational Time

Reduction of the computational time is desirable in any recognition and discrimination process. Low computational costs are very helpful in recognition of images with big size and

Fig. 11 Collection of 12 Selected gray-level images of Mugs

Fig. 12 Collection of 10 Selected gray-level images of Bottles

the discrimination between similar images and shapes from huge image databases. In order to prove the computational efficiency of the proposed method, numerical experiments are conducted using popular image databases.

The first image database is ORL-faces database [24]. This database contains ten different images for the face of each person. The total number of images is equal to 400. All images of this database have the size 92×112. Figure 9 displays a collection of the 40 faces.

The second image database is the Columbia Object image Library (COIL-20) database [25]. The total number of images is 1440 distributed as 72 images for each object. All images of this database have the size 416×448. Figure 10 displays a collection of the 20 objects.

The third and the fourth numerical experiments are conducted using gray-level images of mugs as displayed in Fig. 11 and bottles as displayed in Fig. 12. These images are selected from the ETHZ shape database [26]. All of the selected images are resized to be defined with a unified size equal to 480×480.

The execution-time improvement ratio (ETIR) [27] is used as a criterion to compare the different computational methods. This ratio is defined as $\text{ETIR} = (1 - Time1/Time2) \times 100$, where $Time1$ and $Time2$ are the execution time of the first and the second methods. ETIR = 0 if both execution times are identical.

All numerical experiments are performed using *Sony Vaio E-series* Laptop Machine equipped with Intel® Core i5 CPU

Table 6 Average CPU time and ETIR for selected image databases

Database	Liao's method [28]	Proposed method	ETIR (%)
ORL-faces [24]	0.0501	0.0401	80.04
COIL-20 [25]	0.3267	0.0695	78.70
Bottles [26]	0.3212	0.0709	77.92
Mugs [26]	0.2196	0.0498	77.32

2.7 GHz and 4 GB RAM and operated by 64 bit Windows 8 professional where the executed codes are designed using Matlab7.7.

Low-order GMIs for the selected images are computed by using the method of Liao [28] and the proposed method. The computational processes are performed and repeated 10 times for each of the selected images where the average CPU elapsed times and the execution-time improvement ratio (ETIR) are included in Table 6. It is clear that the proposed method reduced the execution time by 80 % which will be useful in the processing of large size images and shapes.

5 Conclusion

A new set of Gegenbauer moment invariants was constructed for pattern recognition applications. Invariance of the Gegenbauer moments with respect to geometric transformations was verified where the binary- and gray-level images are elongated, contracted and rotated with different transformation factors. The numerical values of the Gegenbauer moment invariants of low orders for original and transformed images are almost the same, which ensure the accuracy of these invariants.

The ability of discriminating between similar images and shapes was tested where these invariants successfully discriminate between similar binary shapes and gray-level images of trademarks.

With respect to the steady growing of digital contents of databases, discriminating the similar images/shapes from these very large scale databases is a big challenge. Extremely fast and highly accurate orthogonal Gegenbauer moment invariants are very useful for online applications.

Content-based images retrieval is a famous approach. This approach is based on computing the features of the digital images and then retrieving the specific image from the database. Implementation of orthogonal Gegenbauer moment invariants will be good choice for future work with very large databases and online applications of digital image retrieval.

References

1. Hu, M.K.: Visual pattern recognition by moment invariants. IRE Trans. Inf. Theory **8**(1), 179–187 (1962)
2. Teague, M.R.: Image analysis via the general theory of moments. J. Opt. Soc. Am. **70**(8), 920–930 (1980)
3. Teh, C.H.; Chin, R.T.: On image analysis by the method of moments. IEEE Trans. Pattern Anal. Mach. Intell. **10**(4), 496–513 (1988)
4. Abramowiz, M.; Stegun, I.A.: Hand Book of Mathematical Functions. Dover Publications, New York (1965)
5. Pawlak, M.: Image Analysis by Moments: Reconstruction and Computational Aspects. Oficyna Wydawnicza Politechniki Wroc_lawskiej, Wroclaw (2006)
6. Hosny, K.M.: Image representation using accurate orthogonal Gegenbauer moments. Pattern Recognit. Lett. **32**(6), 795–804 (2011)
7. Kan, C.; Srinath, M.D.: Invariant character recognition with Zernike and orthogonal Fourier–Mellin moments. Pattern Recognit. **35**, 143–154 (2002)
8. Jazzar Muhanad, M.; Muhammad, G.: Feature selection based verification/identification system using fingerprints and palm print. Arab. J. Sci. Eng. **38**(4), 849–857 (2013)
9. Chong, C.-W.; Paramesran, R.; Mukundan, R.: Translation and scale invariants of Legendre moments. Pattern Recognit. **37**, 119–129 (2004)
10. Srinivasa Rao, Ch.; Srinivas Kumar, S.; Chandra Mohan, B.: Content based image retrieval using exact legendre moments and support vector machine. Int. J. Multimed. Appl. **2**, 69–79 (2011)
11. Pang, Y.-H.; Jin, A.T.B.; Ling, D.N.C.: Enhanced pseudo Zernike moments in face recognition. IEICE Electron. Express **2**(3), 70–75 (2005)
12. Kanan, H.R.; Faez, K.; Gao, Y.: Face recognition using adaptively weighted patch PZM array from a single exemplar image per person. Pattern Recognit. **41**(12), 3799–3812 (2008)
13. Kanan, H.R.; Faez, K.: GA-based optimal selection of PZMI features for face recognition. Appl. Math. Comput. **205**(2), 706–715 (2008)
14. Hosny, K.M.: Exact and fast computation of geometric moments for gray level images. Appl. Math. Comput. **189**(2), 1214–1222 (2007)
15. Hosny, K.M.: Fast and accurate method for radial moment's computation. Pattern Recognit. Lett. **31**(2), 143–150 (2010)
16. Hosny, K.M.: Exact Legendre moment computation for gray level images. Pattern Recognit. **40**(12), 3597–3605 (2007)
17. Hosny, K.M.: A systematic method for efficient computation of full and subsets Zernike moments. Inf. Sci. **180**, 2299–2313 (2010)
18. Hosny, K.M.: Fast and low-complexity method for exact computation of 3D Legendre moments. Pattern Recognit. Lett. **32**, 1305–1314 (2011)
19. Hosny, K.M.; Hafez, M.A.: An algorithm for fast computation of 3D Zernike moments for volumetric images. Math. Problems Eng. **2012**, 1–17. Article ID 353406
20. Available at: http://www.cis.temple.edu/ylatecki/TestData/mpeg7shapeB.tar.gz
21. Wang, B: Shape retrieval using combined Fourier features. Opt. Commun. **284**, 3504–3508 (2011)
22. Mukundan, R.; Ramakrishnan, K.R.: Moment Functions in Image Analysis. World Scientific Publisher, Singapore (1988)
23. United States Patent and Trademark Office, US, Trademark Law, USPTO (2010)
24. http://www.cl.cam.ac.uk/research/dtg/attarchive/facedatabase.html
25. http://www.cs.columbia.edu/CAVE/software/softlib/coil-20.php
26. http://www.vision.ee.ethz.ch/datasets/index.en.html
27. Hosny, K.M.: Fast computation of accurate Zernike moments. J. Real Time Image Process. **3**(1), 97–107 (2008)
28. Liao, S.; Chiang, A.; Lu, Q.; Pawlak, M.: Chinese character recognition via Gegenbauer moments. Proc. IEEE 16th Int. Conf. Pattern Recognit. **3**, 485–488 (2002)